ResearchGate

See discussions, stats, and author profiles for this publication at: https://www.researchgate.net/publication/317247100

Radiological properties of 3D printed materials in kilovoltage and megavoltage photon beams

Article *in* Physica Medica · June 2017

DOI: 10.1016/j.ejmp.2017.05.051

CITATIONS
93

READS
2,848

5 authors, including:

Orrie Lee Dancewicz
Royal Brisbane Hospital
1 PUBLICATION **93** CITATIONS
SEE PROFILE

Steven R. Sylvander
Royal Brisbane Hospital
19 PUBLICATIONS **239** CITATIONS
SEE PROFILE

Tim Markwell
Icon Cancer Centre
26 PUBLICATIONS **182** CITATIONS
SEE PROFILE

Scott Crowe
Royal Brisbane Hospital
144 PUBLICATIONS **1,490** CITATIONS
SEE PROFILE

All content following this page was uploaded by Tim Markwell on 26 November 2017.

The user has requested enhancement of the downloaded file.

Physica Medica 38 (2017) 111–118

Contents lists available at ScienceDirect

Physica Medica

journal homepage: http://www.physicamedica.com

Original paper

Radiological properties of 3D printed materials in kilovoltage and megavoltage photon beams

O.L. Dancewicz [a,b,*], S.R. Sylvander [c], T.S. Markwell [d], S.B. Crowe [a,c], J.V. Trapp [a]

[a] School of Chemistry, Physics and Mechanical Engineering, Queensland University of Technology, Brisbane 4000, Australia
[b] Department of Nuclear Medicine and Specialised PET Services Queensland, Royal Brisbane and Women's Hospital, Herston 4029, Australia
[c] Cancer Care Services, Royal Brisbane and Women's Hospital, Herston 4029, Australia
[d] Radiation Oncology Mater Center, South Brisbane 4101, Australia

ARTICLE INFO

Article history:
Received 2 September 2016
Received in Revised form 3 May 2017
Accepted 4 May 2017

Keywords:
Radiotherapy
3D printing
Computed tomography
Radiological properties

ABSTRACT

Purpose: This study evaluates the radiological properties of different 3D printing materials for a range of photon energies, including kV and MV CT imaging and MV radiotherapy beams.
Methods: The CT values of a number of materials were measured on an Aquilion One CT scanner at 80 kVp, 120 kVp and a Tomotherapy Hi Art MVCT imaging beam. Attenuation of the materials in a 6 MV radiotherapy beam was investigated.
Results: Plastic filaments printed with various infill densities have CT values of −743 ± 4, −580 ± 1 and −113 ± 3 in 120 kVp CT images which approximate the CT values of low-density lung, high-density lung and soft tissue respectively. Metal-infused plastic filaments printed with a 90% infill density have CT values of 658 ± 1 and 739 ± 6 in MVCT images which approximate the attenuation of cortical bone. The effective relative electron density RED_{eff} is used to describe the attenuation of a megavoltage treatment beam, taking into account effects relating to the atomic number and mass density of the material. Plastic filaments printed with a 90% infill density have RED_{eff} values of 1.02 ± 0.03 and 0.94 ± 0.02 which approximate the relative electron density *RED* of soft tissue. Printed resins have RED_{eff} values of 1.11 ± 0.03 and 1.09 ± 0.03 which approximate the *RED* of bone mineral.
Conclusions: 3D printers can model a variety of body tissues which can be used to create phantoms useful for both imaging and dosimetric studies.
Crown Copyright © 2017 Published by Elsevier Ltd on behalf of Associazione Italiana di Fisica Medica. All rights reserved.

1. Introduction

3D printing, also known as additive manufacturing or rapid prototyping, allows models to be built in a matter of hours from simple computer-generated instructions [1,2]. It has sparked a great interest and research effort in the radiotherapy community because of the ability to manufacture custom made phantom materials quickly and often for a fraction of the price of commercial phantoms. The level of detail and accuracy with which models can be printed is high – modern printers can achieve layer thicknesses of tens of microns and sub-millimeter accuracy [3]. With the wide range of 3D printing raw materials available today, such as plastic and resins, the mechanical and structural stability of 3D printed parts is comparable to that of commercial phantom materials.

Many different 3D printing technologies exist today, with two of the most common being Fused Deposition Modeling (FDM) and Stereolithography (SLA) [4]. FDM is a technique where a thermoplastic is melted and extruded onto a platform to create the individual layers of a model [4,5]. The thermoplastics that are used are typically Acrylonitrile Butadiene Styrene (ABS) and Polylactic Acid (PLA), although printing with other materials, such as wood and metal, is also possible. In FDM, the filament is typically extruded in a grid or honeycomb structure, so that even the highest infill density prints contain air gaps on a sub-millimeter scale. While this has previously been identified as a weakness of the FDM printing process [3], the air gaps contained in these models do not make them unusable for radiation dosimetry, and can allow the modeling of low density tissue such as lung [6].

SLA printers use a photopolymer resin which is cured by an ultraviolet laser to form the layers of the model [4,5,7]. Multiple

* Corresponding author at: Department of Nuclear Medicine and Specialised PET Services Queensland, Royal Brisbane and Women's Hospital, Herston 4029, Australia.
E-mail address: odancewicz@gmail.com (O.L. Dancewicz).

http://dx.doi.org/10.1016/j.ejmp.2017.05.051
1120-1797/Crown Copyright © 2017 Published by Elsevier Ltd on behalf of Associazione Italiana di Fisica Medica. All rights reserved.

resin types have also been developed to produce models with varying characteristics such as strength and flexibility. Models printed with SLA printers typically have a 100% infill density and do not contain air gaps. SLA printers are able to print with a higher layer resolution and accuracy than FDM printers [3].

These 3D printing techniques have been widely applied to a number of situations in medical physics including patient-specific dosimetry [8–10]. Brachytherapy moulds have been printed using a low-cost 3D printer, resulting in good catheter positioning accuracy and reproducibility [11]. Proton therapy beam modulation and range compensation has been successfully performed with 3D printed materials [12,13]. 3D printing has also been used in the development of nuclear medicine and imaging phantoms [14,15], the assessment of anatomical noise in computed tomography (CT) image reconstruction algorithms [16,17], and radiation protection [18,19].

The aim of this study is to evaluate the radiological properties of various 3D printing materials for a range of photon energies. An SLA printer is used to print models with an infill density of 100% which can be used to model the attenuation of bone. The SLA technique is compared to the FDM technique, and both are characterized in terms of which tissue types they are able to model. While previous investigations into FDM printing have only used plastics such as ABS and PLA, this study uses metal and wood filaments to model a wider range of tissues.

2. Materials and methods

2.1. CT insert phantom construction

The first aim of the study was to print out phantom inserts that could accurately model the attenuation of various body tissues. Inserts of the Gammex Model 467 Tissue Characterization Phantom. (Gammex Inc., Middleton, USA) were designed and printed using three FDM printers and one SLA printer, listed in Table 1. The Gammex phantom was chosen as it is a widely used phantom in the commissioning and calibration of CT scanners for radiotherapy planning. Phantom inserts include those for water, solid water, lung, adipose, breast, brain, liver and bone [20].

The 3D printing process involves designing the model in a 3D modeling program, exporting this model to the STL (STereoLithography) file format, and uploading the STL file into a slicing program. The slicing software generates the g-code which contains the instructions on the layering of the model and controls other printing parameters such as infill pattern and density. The g-code can then be transferred to the printer, usually via USB memory stick or USB cable.

All insert models were designed using Sketchup Make (Trimble Navigation Limited, Sunnyvale, USA). The inserts were designed with a diameter of 2.7 cm ± 0.05 cm and a length of 7 cm ± 0.05 cm. Four different slicing programs were used to prepare the models for printing, corresponding to the four different printers used: Axon v2.1.0 (3D Systems Inc., Rock Hill, USA), MakerBot® Desktop Beta v 3.9.2 (MakerBot Industries, LLC, Brooklyn, USA), Cura v15.06 (Ultimaker BV., Geldermalsen, The Netherlands) and Preform v1.9.1 (Formlabs Inc., Somerville, USA). The inserts that were printed with the FDM printers were designed with line and grid infill patterns as they were found to take less time to print than the other available fill patterns (honeycomb, circular) and resulted in structurally stable prints. Two different layer heights were used here – 0.50 mm and 0.25 mm. The inserts printed with the SLA printer used a fully enclosed infill and a layer height of 0.05 mm. Infill densities for these printed inserts were chosen to replicate the mass densities of common body tissues (see Table 1).

The thermoplastics printed using the FDM technique were standard ABS, standard PLA, photoluminescent PLA, woodfill, bronzefill and copperfill plastic filament. The bronzefill and copperfill filaments are blends of bronze and copper powder in PLA plastic [21,22]. The woodfill filament is a polymer blend based on PLA and contains wood fibers [23]. The inserts were printed with three different printers: the 3D Touch (3D Systems Inc., Rock Hill, USA), Replicator 2 (MakerBot Industries, LLC, Brooklyn, USA) and the Lulzbot TAZ 5 (Aleph Objects, Inc., Loveland, USA). The Lulzbot TAZ 5 uses a heated bed for extra adherence of the model to the bed during printing. For printing with ABS, the bed is heated to 110 °C and for printing with PLA, it is heated to 60 °C. The estimated size of the air gaps contained within the printed inserts of infill densities 10%-90% is shown in Table 2. Inserts were also printed with the Form 1 + SLA printer (Formlabs Inc., Somerville, USA) using standard and flexible photopolymer resin (see Table 1). The flexible resin is designed for applications where increased impact resistance or compressibility is required [24].

2.2. CT imaging

CT imaging was carried out of the printed inserts in the Gammex phantom along with some of the standard Gammex tissue-equivalent inserts for comparison. The Gammex inserts that were scanned were: water, solid water, lung-300, lung-450, adipose, breast, liver, bone mineral, inner bone, 30% $CaCO_3$, 50% $CaCO_3$ and cortical bone.

The certified CT values in Hounsfield Units (HU) of each insert as measured by a GE CT/i™ scanner (General Electric Healthcare, Boston, USA) are listed in the Gammex phantom user manual [20]. These inserts were used to obtain a Hounsfield Unit (HU) to

Table 2
Air gap size for infill densities of 10%-90%.

Infill density (%)	Air gap size (mm)
10	5.00 ± 0.25
30	3.00 ± 0.15
50	1.00 ± 0.05
70	0.50 ± 0.03
90	0.05 ± 0.01

Table 1
Printing materials, parameters, slicing software and printers used for printing inserts for CT imaging. The Form 1+ printer uses the SLA technique and all other printers use the FDM technique.

Print material	Layer height (mm)	Infill pattern	Infill density (%)	Slicing software	Printer
ABS	0.50	Line	90, 70, 50, 30, 10	Axon v2.1.0	3D Touch
PLA	0.50	Line	90, 70, 50, 30, 10	Axon v2.1.0	3D Touch
Photoluminescent PLA	0.25	Grid	90, 50, 30	Cura v15.06	Lulzbot TAZ 5
Woodfill	0.50	Line	90	MakerBot® Desktop Beta v 3.9.2	Replicator 2
Copperfill	0.50	Line	90	MakerBot® Desktop Beta v 3.9.2	Replicator 2
Bronzefill	0.50	Line	90	MakerBot® Desktop Beta v 3.9.2	Replicator 2
Standard photopolymer resin	0.05	–	100	Preform v1.9.1	Form 1 +
Flexible photopolymer resin	0.05	–	100	Preform v1.9.1	Form 1 +

mass density (CT-D) and HU to electron density (CT-ED) calibration. Kilovoltage CT (kVCT) imaging was performed with a Toshiba Aquilion One CT scanner (Toshiba Medical Systems Corporation, Otawara, Japan) at peak tube potentials of 80kVp and 120kVp, with an exposure of 240 mAs. Megavoltage CT (MVCT) images were also obtained with a Tomotherapy Hi-Art unit (TomoTherapy, Madison, USA), which has a peak imaging beam energy of 3.5 MVp [25]. A 2 mm slice thickness was chosen for all CT images as this is the minimum slice thickness on the Tomotherapy Hi-Art unit. The native resolution of the scanners was used, which corresponds to a pixel size of 1.37 mm × 1.37 mm for the kVCT images and 0.76 mm × 0.76 mm for the MVCT images. An FC09 convolution filter was used with a reconstruction field of view of 700 mm for the kVCT images. The Gammex phantom consists of an inner circle and an outer circle of insert holes, at distances of 5.5 cm and 10.5 cm from the center of the phantom [20]. Each insert was imaged first in the inner circle and then in the outer circle to account for any off-axis variation in the CT value. The setup of the insert in the Gammex phantom is illustrated in Fig. 1. Additional images were taken with the metallic inserts removed from the phantom and replaced with solid water. This was done in order to avoid beam hardening artifacts from the metallic inserts [26,27]. The CT images were analyzed using ImageJ (National Institute of Health, Bethesda, USA). The average of three central slices was taken. The largest possible region of interest (ROI) was chosen that was larger than the air gaps and that excluded the outer boundary of the inserts. This ensured that an average CT value representative of the macroscopic structure of the printed insert was obtained. The ROI size was approximately 314 ± 10 mm^2 for all CT images.

2.3. Slab phantom construction

The second aim of the study was to estimate the radiological thickness of various printing materials. Selected materials were printed as square slabs of 5 cm × 5 cm and variable thicknesses using the settings, software and printers listed in Table 1. The materials printed here were 50% ABS, 50% PLA, woodfill, 90% ABS, 90% PLA, standard photopolymer resin, flexible photopolymer resin, copperfill and bronzefill. The physical thickness of each slab, t, was scaled according to the mass density of the material, ρ, in order to produce approximately the same amount of attenuation as 20 mm of water (Table 3). The mass density ρ was obtained

Table 3
Slab physical thickness, t, printed for radiological thickness calibration. Water is included as a baseline for radiological thickness to which all other slabs were scaled according to mass density ρ. The mass densities of the metallic insert were obtained from the CT-D calibration curve derived from the MVCT images. Mass densities of all other inserts were derived from the kVCT image acquired at 120 kVp.

Material	ρ (g/cm^3)	t (mm)
Bronzefill	1.83 ± 0.04	10.99 ± 0.25
Copperfill	1.73 ± 0.04	11.56 ± 0.25
Standard photopolymer resin	1.07 ± 0.01	19.05 ± 0.03
Flexible photopolymer resin	1.07 ± 0.01	19.05 ± 0.03
90% PLA	1.04 ± 0.03	19.80 ± 0.25
Water	*1.00*	*20.00*
90% ABS	0.90 ± 0.04	22.47 ± 0.25
Woodfill	0.54 ± 0.02	37.74 ± 0.25
50% PLA	0.55 ± 0.05	37.74 ± 0.25
50% ABS	0.43 ± 0.04	47.62 ± 0.25

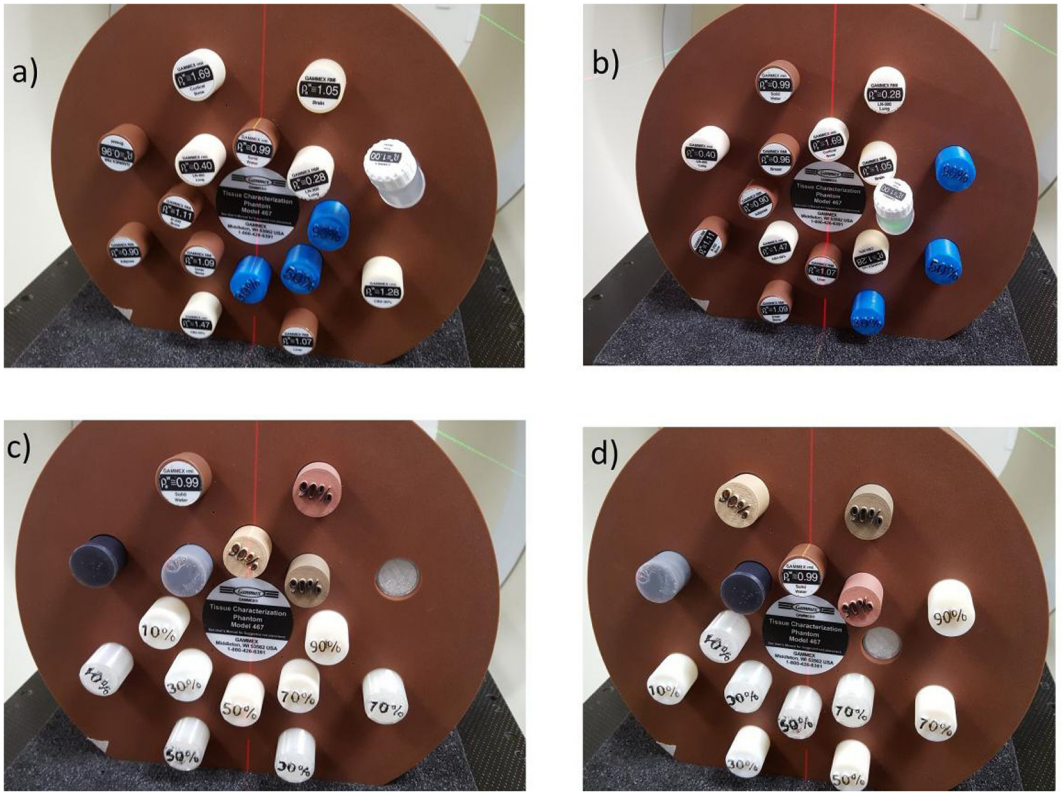

Fig. 1. Setup of the commercial and printed inserts in the Gammex phantom. a) (inner circle, clockwise from 12 o'clock) Solid Water, Lung-300, 90% Photoluminescent PLA, 50% Photoluminescent PLA, 30% Photoluminescent PLA, Inner Bone, Bone Mineral, Lung-450, (outer circle, clockwise from 12 o'clock) Brain, Water, 30% $CaCO_3$, Liver, 50% $CaCO_3$, Adipose, Breast, Cortical Bone. b) outer and inner inserts switched. c) (inner circle, clockwise from 12 o'clock) Woodfill, Bronzefill, 90% ABS, 70% ABS, 50% ABS, 30% ABS, 10% ABS, Standard resin, (outer circle, clockwise from 12 o'clock) Copperfill, 90% PLA, 70% PLA, 30% PLA, 50% PLA, 10% PLA, Flexible resin, Solid Water. d) outer and inner inserts switched.

from the CT-D calibration curve derived from the kVCT image acquired at 120 kVp, except for the metallic inserts, where the MVCT image was used to obtain ρ (see Results). The baseline of 20 mm of water was chosen so that all dose measurements would fall past the depth of maximum dose, d_{max}, (ie. not in the dose buildup region).

2.4. Radiological thickness measurement

Measurements of the dose downstream of the slab were first performed with the material slab alone in the beam, and then with 3.0 cm of solid water placed on the top of the slab (Fig. 2). The two setups were used in order to ensure reproducibility of measurements at two different depths. 100 MU was delivered using a 6 MV beam from a Varian Clinac 21iX (Varian Medical Systems, Palo Alto, USA) and a 3 cm × 3 cm square field. When measuring the attenuation of radiation by an object, a narrow beam geometry is desired [28]. The 3 cm × 3 cm square field provided a narrow beam while also being larger than the chamber volume, thus no detector edge effects were seen. Dose measurements were performed with a pinpoint 3D ionization chamber (PTW 31016, PTW, Freiburg, Germany), which had previously been calibrated against a national standards laboratory. To verify the stability of the chamber signal within the time frame of the measurement, the signal was measured with a 10 cm × 10 cm square field at the start and the end of the measurements.

A tissue maximum ratio (TMR) calibration was performed using the same pinpoint chamber and source-to-detector distance (SDD) as for the slab measurements. The chamber signal downstream of each material slab was used to obtain the water equivalent radiological thickness of the slab, w, (equivalent to 20 mm of water). This was divided by the physical thickness t to arrive at an "effective" relative electron density RED_{eff}. This factor was introduced by Moutrie et al. [29] to describe the attenuation of a specific radiation beam by an object. While electron density-dependent Compton scattering is the main source of attenuation in megavoltage photon beams, RED_{eff} recognizes that atomic number-dependent processes will also have an influence on the attenuation of the beam. The adequacy of RED_{eff} was tested by comparing it to the relative electron density RED of the printed materials and the Gammex inserts as derived from the CT images.

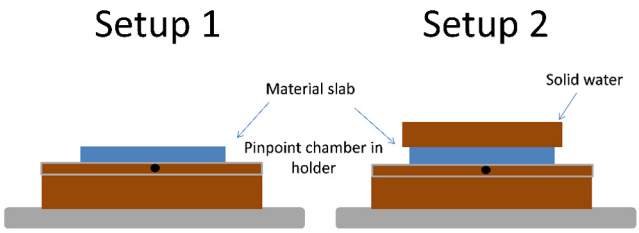

Fig. 2. Experimental setup for radiological thickness measurement.

3. Results

3.1. CT imaging

Fig. 3 shows the 80 kVp and 120 kVp images of the Gammex phantom with the commercial and printed inserts arranged as shown in Fig. 1 a) and c). The copperfill and bronzefill inserts clearly show streaking artifacts.

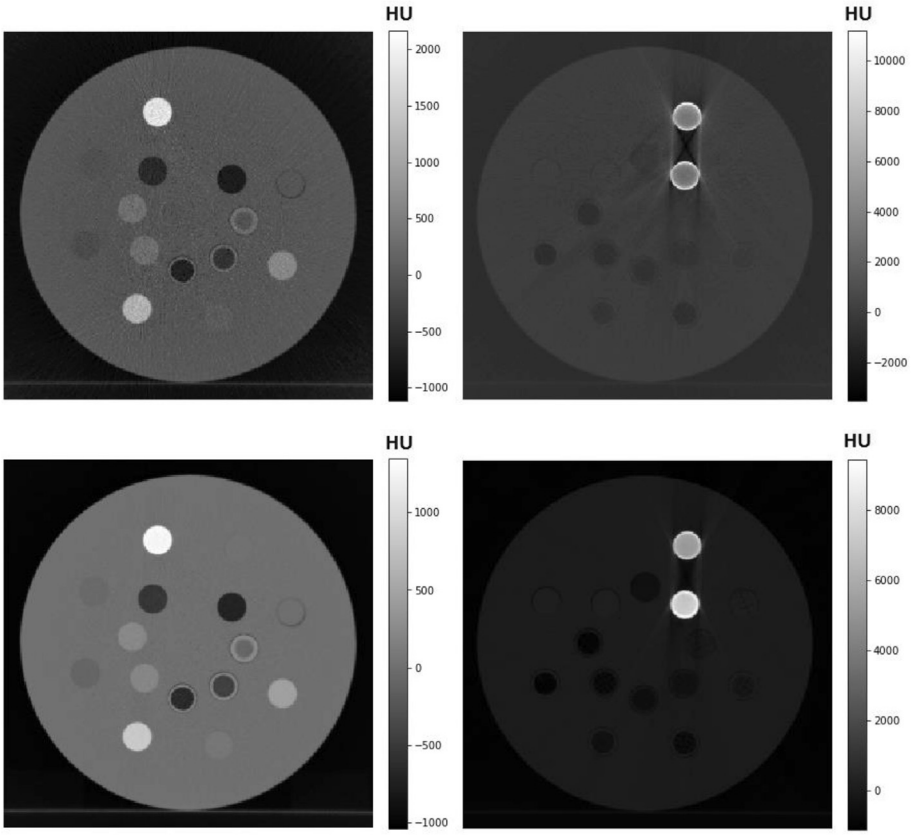

Fig. 3. CT images of Gammex phantom with inserts. From top left: Commercial inserts with photoluminescent PLA printed inserts imaged at 80 kVp, other printed inserts imaged at 80 kVp, Commercial inserts with photoluminescent PLA printed inserts imaged at 120 kVp. Other printed inserts imaged at 120 kVp. Note the streaking artifacts from the copperfill and bronzefill printed inserts.

Tables 4–6 shows a comparison between the CT values of the commercial Gammex inserts and the printed inserts for the kVCT acquisitions at 80 kVp and 120 kVp and the MVCT acquisition.

Table 4
Comparison of CT values of the Gammex inserts and the printed inserts for the kVCT image acquired at 80 kVp. Photo-PLA – Photoluminescent PLA.

Gammex insert	CT value (HU)	Printed insert	CT value (HU)
		10% ABS	−926 ± 14
		10% PLA	−943 ± 14
Lung-300	−746 ± 19	30% ABS	−760 ± 13
		30% PLA	−694 ± 10
		30% Photo-PLA	−673 ± 13
Lung-450	−553 ± 15	50% ABS	−596 ± 22
		Woodfill	−475 ± 14
Adipose	−147 ± 3	50% PLA	−461 ± 3
Breast	−92 ± 7	50% Photo-PLA	−455 ± 22
Water	−22 ± 22	70% ABS	−417 ± 17
Solid Water	−10 ± 7	70% PLA	−228 ± 1
Brain	17 ± 17	90% ABS	−147 ± 18
Liver	57 ± 6	90% PLA	−36 ± 7
Inner Bone	306 ± 10	90% Photo-PLA	−36 ± 8
Bone Mineral	319 ± 2	Flexible resin	33 ± 10
30% $CaCO_3$	622 ± 10	Standard resin	40 ± 11
50% $CaCO_3$	1190 ± 15	Copperfill	3575 ± 475
Cortical Bone	1822 ± 20	Bronzefill	3568 ± 532

Table 5
Comparison of CT values of the Gammex inserts and the printed inserts for the kVCT image acquired at 120 kVp. Photo-PLA – Photoluminescent PLA.

Gammex insert	CT value (HU)	Printed insert	CT value (HU)
		10% ABS	−901 ± 1
		10% PLA	−916 ± 1
Lung-300	−719 ± 11	30% ABS	−743 ± 4
		30% PLA	−688 ± 3
		30% Photo-PLA	−658 ± 14
Lung-450	−533 ± 15	50% ABS	−580 ± 1
		Woodfill	−474 ± 1
Adipose	−88 ± 2	50% PLA	−466 ± 8
Breast	−44 ± 1	50% Photo-PLA	−460 ± 23
Water	−1 ± 1	70% ABS	−408 ± 1
Solid Water	−1 ± 2	70% PLA	−234 ± 5
Brain	22 ± 1	90% ABS	−113 ± 3
Liver	67 ± 6	90% PLA	8 ± 4
Inner Bone	208 ± 9	90% Photo-PLA	−58 ± 1
Bone Mineral	227 ± 14	Flexible resin	98 ± 1
30% $CaCO_3$	524 ± 91	Standard resin	106 ± 1
50% $CaCO_3$	942 ± 146	Copperfill	5372 ± 27
Cortical Bone	1413 ± 213	Bronzefill	7257 ± 24

Table 6
Comparison of CT values of the Gammex inserts and the printed inserts for the MVCT image. Photo-PLA – Photoluminescent-PLA.

Gammex insert	CT value (HU)	Printed insert	CT value (HU)
		10% PLA	−842 ± 1
		10% ABS	−827 ± 1
Lung-300	−668 ± 2	30% ABS	−670 ± 4
		30% Photo-PLA	−615 ± 2
		30% PLA	−606 ± 4
Lung-450	−482 ± 2	50% ABS	−502 ± 4
		50% Photo-PLA	−432 ± 5
Adipose	−44 ± 3	Woodfill	−402 ± 4
Breast	−14 ± 2	50% PLA	−388 ± 3
Solid Water	14 ± 3	70% ABS	−322 ± 5
Water	18 ± 2	70% PLA	−174 ± 1
Brain	65 ± 1	90% Photo-PLA	−91 ± 4
Liver	84 ± 2	90% ABS	−65 ± 4
Inner Bone	120 ± 3	90% PLA	43 ± 1
Bone Mineral	128 ± 6	Flexible resin	143 ± 3
30% $CaCO_3$	284 ± 3	Standard resin	152 ± 7
50% $CaCO_3$	469 ± 5	Copperfill	658 ± 1
Cortical Bone	679 ± 4	Bronzefill	739 ± 6

These CT values represent an average of the measurements at the two radial points of the phantom (average ± standard deviation). There were significant off-axis variations in the CT values of the 30% $CaCO_3$, 50% $CaCO_3$ and Cortical Bone inserts in the CT image acquired at 120 kVp. These amounted to 128 HU ± 12 HU, 206 HU ± 13 HU and 302 HU ± 15 HU respectively. In the CT image acquired at 80 kVp, there were significant off-axis variations in the CT values of the bronzefill and copperfill inserts, amounting to 752 HU ± 454 HU and 647 HU ± 427 HU respectively. There were no significant off-axis variations in the MVCT image (Table 6).

CT-D and CT-ED calibration curves for all printed inserts are shown in Figs. 4 and 5 respectively. The curves are separated into two regions below and above 0 HU corresponding to different slopes and R^2 values.

3.2. Radiological thickness

Table 7 shows the dose chamber signal obtained with the material slabs in both of the setups in Fig. 1, normalized to the solid water signal. The signal measured with a 10 cm × 10 cm square field at the beginning and the end of the measurements was observed to be consistent to within 0.5%. The water equivalent radiological thickness, *w*, as derived from the TMR calibration, and the RED_{eff} of each slab is shown in Table 8.

4. Discussion

4.1. CT imaging

The CT values of the ABS, PLA and photoluminescent PLA printed inserts were observed to increase linearly with infill density when imaged with both kVCT protocols as well as with the MVCT protocol. This corresponds to a linear increase in the mass density and *RED* of the inserts with infill density as well. This effect has been described by Madamesila et al. for a single CT imaging protocol [30]. The current study confirms the linearity of CT value, mass density and *RED* for imaging beams of energies 80 kVp and 120 kVp and also for MVCT.

In the MVCT and 120 kVp images, the CT values of the 90% PLA insert are between the values for water and the brain tissue equivalent insert. In the 80 kVp image, the CT value of the 90% PLA insert is also compatible with the CT value of water within experimental uncertainty. Therefore, at this infill PLA could provide a useful approximation for various types of soft tissue. The CT values of the 90% ABS insert differ from those of the adipose equivalent insert by 0 HU ± 18 HU, 25 HU ± 4 HU and 21 HU ± 5 HU in the 80 kVp, 120 kVp and MVCT images respectively. Thus, ABS printed with an infill density of 90% is a good approximation of adipose tissue. The differences between the CT values of the 50% ABS and the lung-450 inserts are 7% ± 5%, 8% ± 3% and 4% ± 1% in the 80 kVp, 120 kVp and MVCT images respectively. The differences between the CT values of the 30% ABS and the lung-300 inserts are 2% ± 3%, 3% ± 2% and 0% ± 1% in the 80 kVp, 120 kVp and MVCT images respectively. ABS printed with these infill densities is therefore useful for constructing lung-equivalent phantoms. The 30% and 50% PLA and photoluminescent PLA inserts as well as the woodfill insert also approximate lung tissue, although the CT values of these inserts are greater than that of the ABS inserts.

The inserts printed with the standard and flexible photopolymer resins provide good surrogates for bone tissue in the MVCT images. For the 120 kVp and 80 kVp images however, the CT values of these resins are shifted downwards so that they match those of the liver tissue insert rather than the bone inserts. The copperfill and bronzefill inserts are good substitutes for cortical bone in the MVCT scans. However, as shown in Tables 4 and 5 the displayed

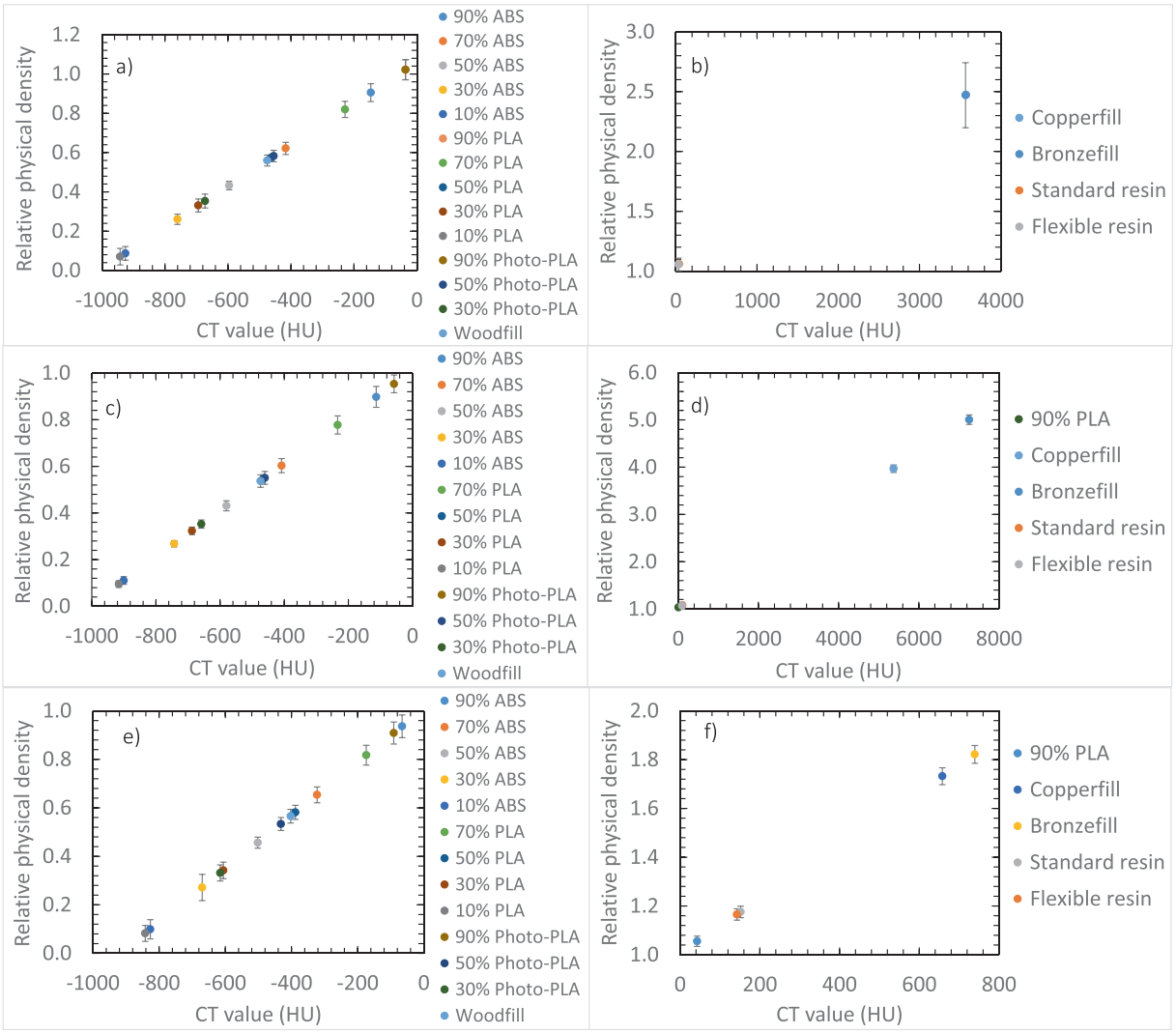

Fig. 4. CT-D calibration curves of the printed inserts. a) 80 kVp image, <0 HU (slope 0.0011 $HU^{-1} \pm 0.0001$ HU^{-1}, $R^2 = 1.00$) b) 80 kVp image >0 HU (slope = 0.0004 $HU^{-1} \pm 0.0001$ HU^{-1}, $R^2 = 1.00$) c) 120 kVp image <0 HU (slope = 0.0010 $HU^{-1} \pm 0.0001$ HU^{-1}, $R^2 = 1.00$) d) 120 kVp image >0 HU (slope = 0.0005 $HU^{-1} \pm 0.0001$ HU^{-1}, $R^2 = 0.91$) Photo-PLA – Photoluminescent PLA. e) MVCT image <0 HU (slope = 0.0011 $HU^{-1} \pm 0.0001$ HU^{-1}, $R^2 = 1.00$) f) MVCT image >0 HU (slope = 0.0011 $HU^{-1} \pm 0.0001$ HU^{-1}, $R^2 = 1.00$). Photo-PLA – Photoluminescent PLA.

CT values of these metallic inserts in the 80 kVp and 120 kVp images are outside the normal range of −1024 to +3096 for body tissue [31]. This is likely due to artifacts that are usually seen in kVCT images of metallic objects (Fig. 3). Kairn et al. has shown that the CT values of metallic objects themselves are misrepresented in kVCT images [27]. In general, the CT values of the metallic inserts in our 80 kVp and 120 kVp images seem to be overestimated by about 3000–6000 HU. Moreover, the CT-D and CT-ED calibration curves generated from the 80 kVp and 120 kVp images of the Gammex inserts do not include materials with the density of the metallic inserts. Since other effects, such as photoelectric absorption, are present when these inserts are imaged at kV energies and may affect the linearity of the curves, the density of these materials cannot simply be extrapolated from a single linear curve. In the 80 kVp image, the off-axis variations associated with the metallic inserts as well as their errors are quite high. Again, this is likely caused by the large streaking artifacts as well as the noise in the image (Fig. 3, top right pane). On the other hand, the MVCT images do no exhibit any of these artifacts. Thus, 3D printed materials can give a true estimate of the CT value of high-density inserts and implants, such as prosthetics, in MVCT imaging even if these materials contain metals.

The average variation in CT value between the 80 kVp image and the 120 kVp image is similar for the commercial Gammex lung-equivalent inserts and the printed lung-equivalent inserts – 4% and 2% respectively. For soft-tissue equivalent inserts, the average variations in CT values are 54% for the Gammex inserts and 67% for the printed inserts.

4.2. Radiological thickness

For most materials listed in Table 8, *RED* and RED_{eff} are compatible within experimental uncertainty. This is particularly true for the standard resin, flexible resin, 90% PLA, 90% ABS and the woodfill slabs. For the 50% PLA and 50% ABS slabs, the RED_{eff} is higher than the *RED* by 0.12 ± 0.05 and 0.15 ± 0.04 respectively. For the bronzefill and copperfill slabs, the disagreement is worse - the RED_{eff} is higher than the *RED* by 0.47 ± 0.10 and 0.50 ± 0.11 respectively. The RED_{eff} of some of the printed slabs is also compatible with the *RED* of some of the Gammex tissue-equivalent inserts within experimental uncertainty. The standard and flexible resin slabs have a value for RED_{eff} that is between the electron densities for bone mineral and liver. The 90% PLA slab has a RED_{eff} that is between the electron densities of liver and solid water. The 90%

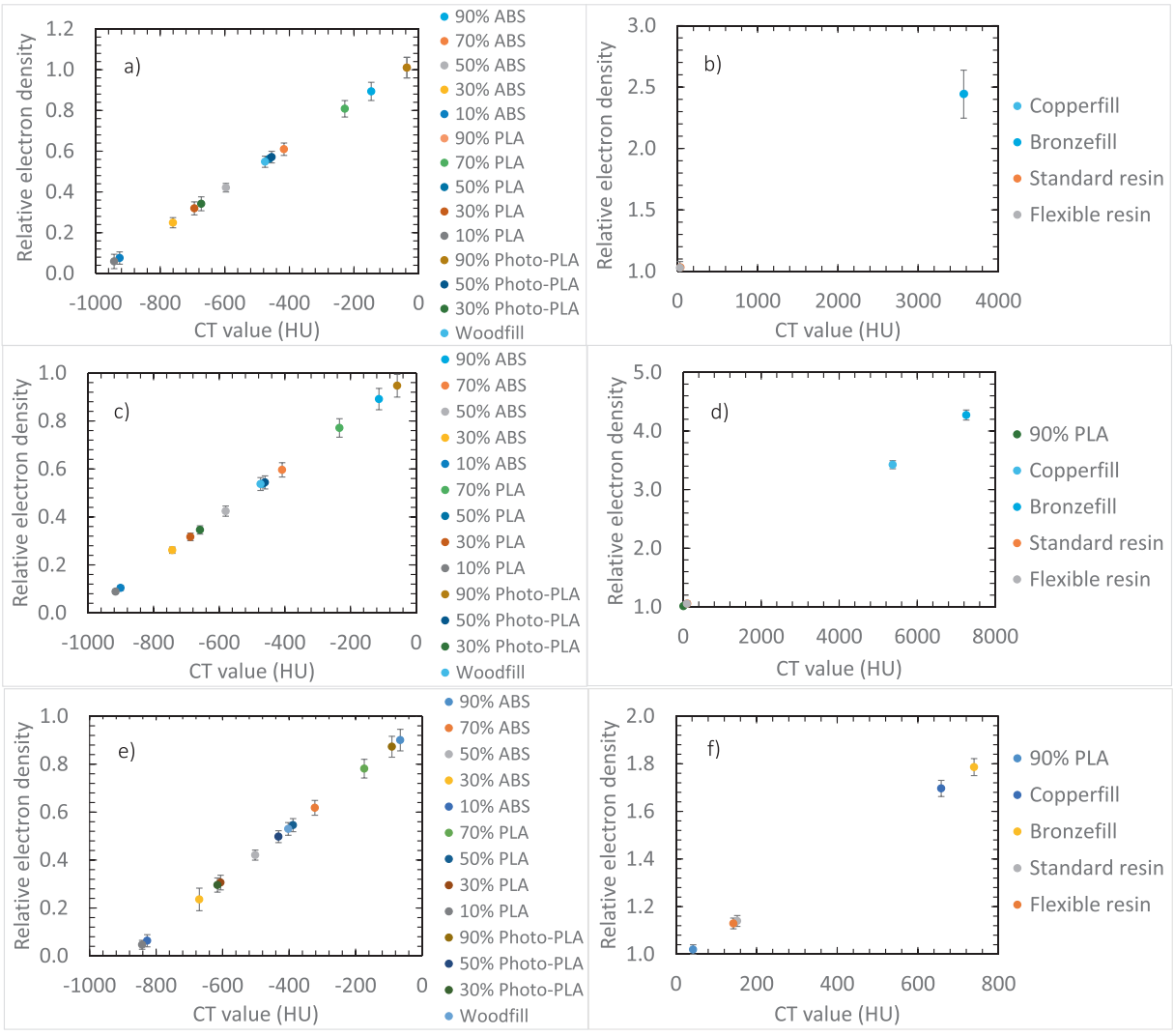

Fig. 5. CT-ED calibration curves of the printed inserts. a) 80 kVp image, <0 HU (slope 0.0011 $HU^{-1} \pm 0.0001$ HU^{-1}, $R^2 = 1.00$) b) 80 kVp image >0 HU (slope = 0.0004 $HU^{-1} \pm 0.0001$ HU^{-1}, $R^2 = 1.00$) c) 120 kVp image <0 HU (slope = 0.0010 $HU^{-1} \pm 0.0001$ HU^{-1}, $R^2 = 1.00$) d) 120 kVp image >0 HU (slope = 0.0005 $HU^{-1} \pm 0.0001$ HU^{-1}, $R^2 = 0.91$) e) MVCT image <0 HU (slope = 0.0011 $HU^{-1} \pm 0.0001$ HU^{-1}, $R^2 = 1.00$) f) MVCT image >0 HU (slope = 0.0011 $HU^{-1} \pm 0.0001$ HU^{-1}, $R^2 = 1.00$). Photo-PLA – Photoluminescent PLA.

Table 7
Chamber signal obtained for each of the material slabs.

	Normalized chamber signal	
Material	Setup 1	Setup 2
Bronzefill	0.979	0.985
Copperfill	0.977	0.986
Standard photopolymer resin	0.993	0.996
Flexible photopolymer resin	0.995	0.998
90% PLA	0.997	0.998
Solid water	1.000	1.000
90% ABS	0.993	0.992
Woodfill	0.997	0.988
50% PLA	0.978	0.971
50% ABS	0.969	0.958

Table 8
Relative electron density derived from CT images, RED, calculated water equivalent radiological thickness, w (equivalent to 20 mm of water), and RED_{eff}, of each material.

Material	*RED*	*w* (mm)	RED_{eff}
Bronzefill	1.79 ± 0.03	24.89 ± 0.07	2.26 ± 0.10
Copperfill	1.70 ± 0.04	25.42 ± 0.08	2.20 ± 0.10
Standard resin	1.06 ± 0.02	21.14 ± 0.06	1.11 ± 0.03
Flexible resin	1.05 ± 0.01	20.78 ± 0.06	1.09 ± 0.03
90% PLA	1.01 ± 0.03	20.24 ± 0.06	1.02 ± 0.03
90% ABS	0.89 ± 0.04	21.14 ± 0.06	0.94 ± 0.02
Woodfill	0.53 ± 0.02	20.24 ± 0.06	0.54 ± 0.01
50% PLA	0.54 ± 0.05	25.06 ± 0.08	0.66 ± 0.01
50% ABS	0.43 ± 0.04	27.39 ± 0.08	0.58 ± 0.01

ABS slab has a RED_{eff} that is between the electron densities of adipose and breast tissue. This demonstrates that, for most materials, the term RED_{eff} is useful for describing the attenuation of a MV treatment beam, taking into account effects not related to electron density. However, there may be some atomic number-dependent effects, such as photoelectric absorption in the case of the metallic slabs, or some mass density-dependent effects, in the case of the low density slabs, that are not completely accounted for [29]. This could explain the large differences between the *RED* and RED_{eff} for these materials.

5. Conclusions

3D printed materials can model a wide variety of body tissues, including lung, adipose, liver, inner bone and cortical bone. These

tissue types are accurately modeled in kVCT and MVCT imaging. Phantoms printed with metallic filaments accurately model cortical bone in MVCT imaging, but are susceptible to the usual beam hardening artifacts as seen with metal objects in kVCT imaging.

The radiological thickness of the materials tested is comparable to that of standard body tissues. The effective relative electron density, RED_{eff}, adequately describes the radiological thickness of most printed materials and the attenuation of a megavoltage treatment beam. This study shows that modern 3D printers can be used to model a variety of body tissues, and that phantoms created in this way are useful for both imaging and dosimetric studies. However, it is important to remember that materials printed with resins and metallic filaments are good surrogates for bone tissue and cortical bone in MVCT only.

Acknowledgments

The authors would like to acknowledge Queensland University of Technology for use of the Lulzbot TAZ 5 and Makerbot Replicator 2, Royal Brisbane and Womens Hospital (RBWH) Department of Nuclear Medicine and Specialised PET Services Queensland for use of the 3D Touch and RBWH Cancer Care Services for use of the Form 1+. The authors would also like to acknowledge Craig Lancaster from RBWH Cancer Care Services for facilitating use of the Tomotherapy unit.

The authors have no relevant conflicts of interest to disclose.

References

[1] Zhai Y, Lados DA, Lagoy JL. Additive manufacturing: making imagination the major limitation. JOM 2014;66:808–16.
[2] Gibson I, Cheung LK, Chow SP, Cheung WL, Beh SL, Savalini M, et al. The use of rapid prototyping to assist medical applications. Rapid Prototyping J 2006;12:53–8.
[3] Leary M, Kron T, Keller C, Franich R, Lonski P, Subic A, et al. Additive manufacture of custom radiation dosimetry phantoms: an automated method compatible with commercial polymer 3D printers. Mater Des 2015;86:487–99.
[4] Kruth J-P, Leu MC, Nagakawa T. Progress in additive manufacturing and rapid prototyping. CIRP Ann Manuf Techn 1998;47:525–40.
[5] Yan X, Gu P. A review of rapid prototyping technologies and systems. Comput Aided Des 1996;28:307–18.
[6] Kairn T, Crowe SB, Markwell T. Use of 3D printed materials as tissue-equivalent phantoms. In World Congress on Medical Physics and Biomedical Engineering 2015, Toronto, Canada: IFMBE Proceedings 51.
[7] Jacobs PF. Fundamentals of stereolithography. In Solid Freeform Fabrication Symposium July 1992:196–211.
[8] Ehler ED, Barney BM, Higgins PD, Dusenbery E. Patient specific 3D printed phantom for IMRT quality assurance. Phys Med Biol 2014;59:5763–73.
[9] Kiarashi N, Nolte AC, Sturgeon GM, Segars WP, Ghate SV, Nolte LW, et al. Development of realistic physical breast phantoms matched to virtual breast phantoms based on human subject data. Med Phys 2015;42:4116–26.
[10] Mayer R, Liacouras P, Thomas A, Kang M, Lin L, Simone II CB. 3D printer generated thorax phantom with mobile tumor for radiation dosimetry. Rev Sci Instrum 2015;86:074301.
[11] Harris BD, Nilsson S, Poole CM. A feasibility study for using ABS plastic and a low-cost 3D printer for patient-specific brachytherapy mould design. Australas Phys Eng Sci Med 2015;38:399–412.
[12] Lindsay C, Kumlin J, Jirasek A, Lee R, Martinez DM, Schaffer P, et al. 3D printed plastics for beam modulation in proton therapy. Phys Med Biol 2015;60:N231–40.
[13] Ju SG, Kim MK, Hong C-S, Kim JS, Han Y, Choi DH, et al. New technique for developing a proton range compensator with use of a 3-Dimensional printer. Int J Radiat Oncol Biol Phys 2014;88:453–8.
[14] Miller MA, Hutchins GD. Development of anatomically realistic PET and PET/CT phantoms with rapid prototyping technology. In 2007 IEEE Nuclear Science Symposium Conference Record 2007, Honolulu, USA:4252–7.
[15] Bieniosek MF, Lee BJ, Levin CS. Technical note: characterization of custom 3D printed multimodality imaging phantoms. Med Phys 2015;42:5913–8.
[16] Solomon J, Samei E. Quantum noise properties of CT images with anatomical textured backgrounds across reconstruction algorithms: FBP and SAFIRE. Med Phys 2014;41:091908.
[17] Solomon J, Ba A, Bochud F, Samei E. Comparison of low-contrast detectability between two CT reconstruction algorithms using voxel-based 3D printed textured phantoms. Med Phys 2016;43:6497–506.
[18] Sato F, Maekawa T, Sakiyama T, Zushi N, Shimizu K, Kato Y, et al. Development of human hand phantom containing radiophotoluminescence material. Radiat Meas 2016;85:18–25.
[19] Zemnick C, Woodhouse SA, Gewanter RM, Raphael M, Piro JD. Rapid prototyping techniques for creating a radiation shield. J Prosthet Dent 2007;97:236–41.
[20] Gammex Inc., Tissue characterization phantom model 467 user's guide; 2004: Middleton, USA.
[21] ColorFabb BV. Bronzefill, http://colorfabb.com/bronzefill; 2016 [accessed 09.02.16].
[22] ColorFabb BV. Copperfill, http://colorfabb.com/copperfill; 2016 [accessed 09.02.16].
[23] ColorFabb BV. Woodfill, http://colorfabb.com/woodfill-fine; 2016 [accessed 09.02.16].
[24] Formlabs, Inc. Flexible photopolymer resin for Form 1+ material properties, http://formlabs.com/media/upload/Flexible-DataSheet.pdf; 2014 [accessed 02.02.16].
[25] Jeraj R, Mackie TR, Balog J, Olivera G, Pearson D, Kapatoes J, et al. Radiation characteristics of helical tomotherapy. Med Phys 2004;31:396–404.
[26] Barrett JF, Keat N. Artifacts in CT: recognition and avoidance. Radiographics 2004;24:1679–91.
[27] Kairn T, Crowe SB, Fogg P, Trapp JV. The appearance and effects of metallic implants in CT images. Australas Phys Eng Sci Med 2013;36:209–17.
[28] Midgley S. Angular width of a narrow beam for X-ray linear attenuation coefficient measurements. Radiat Phys Chem 2006;75:945–53.
[29] Moutrie V, Kairn T, Rosenfeld A, Charles PH. Use of a megavoltage electronic portal imaging device to identify prosthetic materials. Australas Phys Eng Sci Med 2015;38:93–100.
[30] Madamesila J, McGeachy P, Barajas JEV, Khan R. Characterizing 3D printing in the fabrication of variable density phantoms for quality assurance of radiotherapy. Phys Medica 2016;32:242–7.
[31] Michael G. X-ray computed tomography. Phys Educ 2001;36:442–51.

View publication stats